Intrinsic radiation from Poynting jets and magnetized collisionless shocks: implications for prompt GRB emissions

E. P. LIANG and K. NOGUCHI
Rice University, Houston, TX 77005-1892

Summary

We summarize latest PIC simulation results on the radiation from Poynting jets and strongly magnetized collisionless shocks when a Poynting jet runs into cold ambient medium. We find that in all cases the radiative power output is much below that predicted by synchrotron radiation and the critical frequency is also much lower than the synchrotron critical frequency. This is because the accelerations to highest energies are done by forces parallel rather than perpendicular to the momentum. We discuss the implications for the interpretation of GRB prompt emission data.

PACS 98.70.Rz
PACS 01.30.Cc

1. Introduction

Two popular paradigms of GRB energy source are relativistic hydrodynamic (HD) outflows [1], and electromagnetic (EM) or Poynting flux (PF)-dominated outflows [2], driven by the formation of a black hole or magnetar in a collapsar or compact-objects merger. In either paradigm the challenge is to find robust mechanisms which efficiently convert HD or EM energy into the relativistic kinetic energy of nonthermal particles and radiation. A popular model of the HD paradigm is the synchrotron shock model, where unsteady flow leads to dissipation via internal shocks in the prompt phase and snowplowing of the CSM/ISM leads to external shock emission in the afterglow phase. In collisionless shocks (CS), Weibel instability [3] has been invoked to generate turbulent magnetic fields, leading to diffusive electron acceleration followed by "jitter" radiation [4], though inverse Comptonization in dense photon environments [4] has also been suggested. In the PF paradigm, particle acceleration and radiation are driven directly by large-scale EM fields via collective plasma processes [2]. A hybrid scenario is EM-dominated shocks, in which the internal/external shocks are mediated by strong ordered EM fields.

In all scenarios, particle acceleration and radiation ultimately come down to plasma kinetics, which are best modeled using large-scale Particle-in-Cell (PIC) codes [5]. In the past few years, using the most advanced PIC codes, we have performed hundreds of simulations of PF and CS scenarios [6,8]. Here we summarize the latest results on the radiation output of sample PF and CS models. We compute the instantaneous radiation power output of each particle directly from the particle and field data of the PIC simulations using $P_{rad} = 2e^2(F_{\parallel}{}^2 + \gamma^2 F_{+}{}^2)/3c$ where $F_{\parallel}$ is the force parallel to velocity **v** and F_{+} is the force orthogonal to **v** [4], and compare them to GRB data. The most significant finding is that *in both PF and CS models the in-situ radiation from the most energetic particles are far from classical synchrotron radiation, and the typical power output is many orders of magnitudes below that of synchrotron radiation for a given magnetic field and Lorentz factor (in the lab frame). Physically this is because the most efficient acceleration is done by forces parallel to the momentum, whereas synchrotron radiation occurs only when the force is perpendicular to the momentum.* In the PF case, the critical frequency is also much lower than the synchrotron critical frequency. These results have far reaching implications for the interpretation of GRB output and spectra [7].

2 Radiation from PF Models

The physics of direct-drive PF acceleration have been discussed in previous publications [6, 8] and will not be repeated here. (Several powerpoint presentations and movies are available at our websites:http://spacibm.rice.edu/~liang/picsimandhttp://spacibm.rice.edu/~knoguchi). Direct PF acceleration of plasmas fall into two main categories: front-loaded or back-loaded. In the former case, which we will call leading Ponderomotive accelerator (LPA), the EM ponderomotive force snowplows the electrons ahead of it without penetrating beyond the skin depth, as in laboratory laser-target interactions. In this case the PF momentum is shared by all upstream particles, so the Lorentz factor of the particles is limited by $\max(\Omega_e/\omega_{pe}, a_o^2/2)$ where Ω_e is the electron gyrofrequency, ω_{pe} is the electron plasma frequency and a_o =eA/mc is the dimensionless vector potential. In the latter case, which we call trailing Ponderomotive accelerator (TPA, this term replaces the acronym DRPA used in our early publications) the plasma-loaded EM pulse pulls the trailing plasma behind it via self-induced J x B force. The PF continuously accelerate the fastest particles but gradually leave slower particles behind. Decreased plasma loading allows both the PF and residual fast particles to accelerate over time, reaching Lorentz factors far exceeding Ω_e/ω_{pe} or $a_o^2/2$ in our PIC simulations. Ultimately the Lorentz factor is limited by radiation damping or dephasing (self-induced or externally induced). We have studied radiation by both TPA and LPA. For a given input PF amplitude, TPA particles radiates much more broadly than LPA since all particles are imbedded in the strong fields. Even for TPA, P_{rad} is many orders of magnitude below that of classical synchrotron radiation with the same B and γ. This is because the fast TPA particles see a comoving B field. Both the net Lorentz force and particle velocity make only small angles with the Poynting vector. We find that radiation from the comoving TPA particles can be approximated to first order by the analytic formula $P_{analytic} \sim r_o^2 c\, B^2 p_+^2 \sin^2\alpha$, where r_o is classical electron radius, p_+ is total momentum *orthogonal* to the Poynting vector **k** (including component of **p** || to **B**!), and α is the angle between **v** and **k**. Fig.1 compares the numerical P_{rad} versus $P_{analytic}$, showing excellent correlation (the scatter is due to initial momentum terms not included in the above formula). Intuitively, high γ particles are moving mainly along **k**, so $p_+ << \gamma$ and $\sin\alpha << 1$. Hence P_{rad} is << classical synchrotron power $P_{syn} \sim r_o^2 c\, B^2\gamma^2$. Similarly, the comoving B causes only small curvature in the particle tracks. So the critical radiation frequency which is related to the duration of sweep of the photon beam across the observer at infinity [4] can be shown to approximate $\omega_{cr} \sim \Omega_e \gamma^2 \sin^2\alpha$ << the synchrotron critical frequency $\omega_{cr} \sim \Omega_e \gamma^2$.

In all PF models, the late-time P_{rad} asymptotes to a constant value which depends on the initial ejecta temperature and magnetic field. The hotter the initial ejecta, the higher the asymptotic P_{rad} (Fig.2). We find that the asymptotic P_{rad} scales roughly as p_o^2 where p_o is the initial average particle momentum. We also find that the asymptotic P_{rad} scales with initial PF field B_o roughly as B_o^n with n~2-3 (Fig.3). In most PF runs the asymptotic particle spectrum has a power law index near 3.5 (Fig4). This is consistent with the observed gamma-ray spectrum of most high energy sources in the optically-thin non-cooling limit [4].

3. Radiation from CS models

(1). In CS models, P_{rad} is strongly dependent on B at the shock. For transverse EM-dominated shocks (Alfven speed $v_A > c$), we obtain values similar to the PF case for ejecta electrons, but factors of 10 lower for shocked ambient electrons (Fig.5). For weakly magnetized shocks, simulations suggest that similar scaling exists but we have not yet derived an analytic formula.

In nonmagnetic shocks we find that the highest energy particle are mainly accelerated by plasma wave electric fields, not Fermi scattering as had been postulated. In this case P_{rad} is much lower than even the PF formula, when B refers to the downstream turbulent field generated by Weibel instability [3]. This is because the high γ particles are mostly accelerated away from the Weibel-generated field region.

2). In CS models of e+e- shocking e-ion plasmas (Fig.6), we find that the shocked ambient electrons radiate roughly at the same level as in e+e- shocking e+e- plasmas for a given B field of the ejecta.

3). In all magnetized PF and CS cases, the radiation output is strongly linearly polarized as expected [8,9].

4. Implications for prompt GRB emissions

Current models of GRB emissions, whether they are driven by HD or PF, assume that radiation occurs in-situ with the particle acceleration. As we show above, the in-situ radiation in all our PIC simulations are many orders of magnitude below that of synchrotron radiation, for a given local magnetic field and particle Lorentz factor. Physically, this result is not surprising, since the condition is most favorable to achieve the highest energy when the in-situ Lorentz force is most aligned with the particle momentum, whereas synchrotron radiation occurs when the particle momentum is mostly transverse to the Lorentz force. Also the particle momentum distributions in our PIC simulations are highly anisotropic, with the largest component along the Poynting vector in the PF case and normal to the shock front in the CS case. This suggests that particles will lose much less energy per unit distance traveled and achieve much higher Lorentz factors than conventional synchrotron models. Unless these ultrarelativistic particles eventually finds a "beam dump" to convert their energy into synchrotron (if the beam dump is a strongly magnetized plasma) or inverse Compton radiation (if the beam dump is a dense soft photon field), the accelerator will traverse large distances before the HD or PF energy is fully radiated away. On one hand this solves the rapid cooling problem of synchrotron shock models. On the other hand we need to completely revise the emission region parameters which are usually based on the synchrotron model. The results of our PIC simulations suggest that we need to completely revise the "standard" scenario based on alternative emission mechanisms much less efficient than synchrotron radiation. These and other implications for the interpretation of GRB prompt emissions, include the Amati-Ghirlanda relations [10, 11] will be addressed in future papers.

References

1. T. Piran, *Phys. Rep*. **333**, (2000) 529; P. Meszaros, *Ann. Rev. Ast. Astrophys*. **40**, (2002) 137; G. Fishman & C.A. Meegan, *Ann. Rev. Ast. Astrophys*. **33**, (1995) 415; G. Fishman, in *Compton Gamma-Ray Observatory*, edited by M. Friedlander, M. *et al*. *AIP Conf. Proc*. **280**, (Am. Inst. Phys., New York) 1993, p.669; R.D. Preece *et al. Astrophys. J. Supp*. **126**, (2000) 19.

2. See for example M.V. Smolsky and V.V. Usov, *Astrophys. J*. **531**, (2000) 764; M.H.P.M. Van Putten and A. Levinson, *Astrophys. J*. **584**, (2003) 937; A. Levinson and M.H.P.M. Van Putten, *Astrophys. J*. **488**, (1997) 69; M. Lyutikov and R. Blandford, *Proc.1st N. Bohr Summer Inst.,* edited by R.Ouyed *et al* (2003, astroph020671); M. Lyutikov and E.G. Blackman, *MNRAS* **321**, (2002) 177; E.G. Blackman, *Proc.1st N. Bohr Summer Inst*., edited by R.Ouyed et al (2003, astroph0211187).

3 Silva, L.O. *et al*. *ApJ* **596**, (2003) L121; Nishikawa, K. *et al*. *ApJ* **595**, (2003) 555.
4. G. Rybicki & A.P. Lightman, *Radiative Processes in Astrophysics* (Wiley, New York) 1979; Medvedev, M. *ApJ* **540**, (2000) 704; *ibid ApJ* in press (2006).
5. C. K. Birdsall and A. B. Langdon, *Plasma Physics via Computer Simulation*, (IOP, Bristol, UK) 1991; K. Nishimura, S.P. Gary and H. Li, *J. Geophys. Res.* **107**, (2002) 1375; A. B. Langdon, *Comp. Phys. Comm.* **70**, (1992) 447; A.B. Langdon, and B. Lasinski, *Meth. Comp. Phys.***16**, , edited by B. Alder *et al*. (1976) 327.
6. E. Liang *et al*. *Phys. Rev. Lett.* **90**, (2003) 085001; E. Liang and K. Nishimura, *Phys. Rev. Lett*. **92**, (2004) 175005; K. Nishimura and E. Liang, *Phys. Plasmas* **11** (10) (October, 2004); K. Nishimura, E. Liang, and S.P. Gary, *Phys. Plasmas* **10**(11) (2003) 4559.
7. E. Liang & K. Noguchi, *ApJ* to be submitted (2006)
8. E. Liang,, *Astrophys. Sp. Sci*. Proc. HEDLA Workshop, in press (2005); *Adv. Plasma Research*, ed. M. Lyutikov, in press (2005); Chiba Japan Conf. Proc. (2005 www.astro.phys.s.chiba-u.ac.jp/ca2005/); BAPS 50, 113 (2005).
9. K. Noguchi *et al*, *Il Nuovo Cimento* **28C**, (2005 astroph0504612); *Texas Symp. At Stanford Proc*. in press (2005, astroph0504561); *J.Comp.Phys*. to be submitted (2006).
10. L. Amati, *et al. Ast. Ap*. **390**, (2002) 81.
11. G. Ghirlanda *et al. ApJ* **613**, (2004) L13; *ibid, ApJ* **616**, (2004) 331.

Figure captions

Fig.1 Sample scatterplot of radiative power P_{rad} from electrons accelerated by a Poynting jet ($v_{Ao}/c=10$), compared with the analytic formula $P_{analytic} \sim r_o^2 c\, B^2\gamma^2 \sin^4\alpha$, shows good correlation, especially at high P_{rad}. In all figures, we plot only 1/8 of all superparticles used in the simulations. P_{rad} and $P_{analytic}$ are normalized by the same fixed units.

Fig2 Snapshots of P_{rad} vs. distance x (in units of $3c/\omega_{pe}$ for all figures) for Poynting jet accelerated e+e- as the jet expands from grid center (x=36000) to both sides (colors denote increasing times). We show evolutions for initial magnetic field $v_{Ao}/c=10$, but for two different initial jet internal temperatures kT_o (a=5 MeV, b= 5 keV): higher kT_o leads to higher radiative power and broader emission regions at late times.

Fig.3 Snapshots of P_{rad} vs. x as in Fig.2b but different initial magnetic fields v_{Ao}/c ($a=10^2$, $b=10^3$, $c=10^4$). Jets start expansion from grid center (x=180). Colors denote increasing times. Results show that P_{rad} scales as B^n where n~2-3. P_{rad}~constant level at late times, because the decrease in angle α roughly cancels the increase in Lorentz factor γ.

Fig.4 Electron energy spectra from different e+e- Poynting jets show robust power-law index ~ 3.5 independent of the simulation box size. An electron index of ~3.5 is consistent with the photon power-law index of most GRBs, blazars and pulsars [7].

Fig.5(a) Magnetic shock structure when an e+e- Poynting jet ($v_{Ao}/c=10$) sweeps up cold e+e- ambient plasma with density =0.1% of jet. We plot the magnetic field B_y and p_x for ejecta and swept-up e-. B_y is strongly suppressed inside the shock transition region (x=3994-4020). (b) Snapshots of P_{rad} vs. x for the swept-up e- (colors denote increasing time). Note that P_{rad} starts high, goes through a minimum, before recovering to ~ constant level at late times.

Fig.6 (a) Magnetic shock structure when an e+e- Poynting jet ($v_{Ao}/c=10$) sweeps up cold e-ion ambient plasma ($m_i/m_e=100$) with density=0.1% of jet. The shock transition region (x=3920-4020) is broader than that of Fig.5 due to e-ion charge separation. We show snapshots of P_{rad} vs. x for ejecta e- (b) and for swept-up e- (c). Note that the radiating zone in (c) is much broader than in Fig.5, but the magnitude of P_{rad} is similar to that of Fig.5.

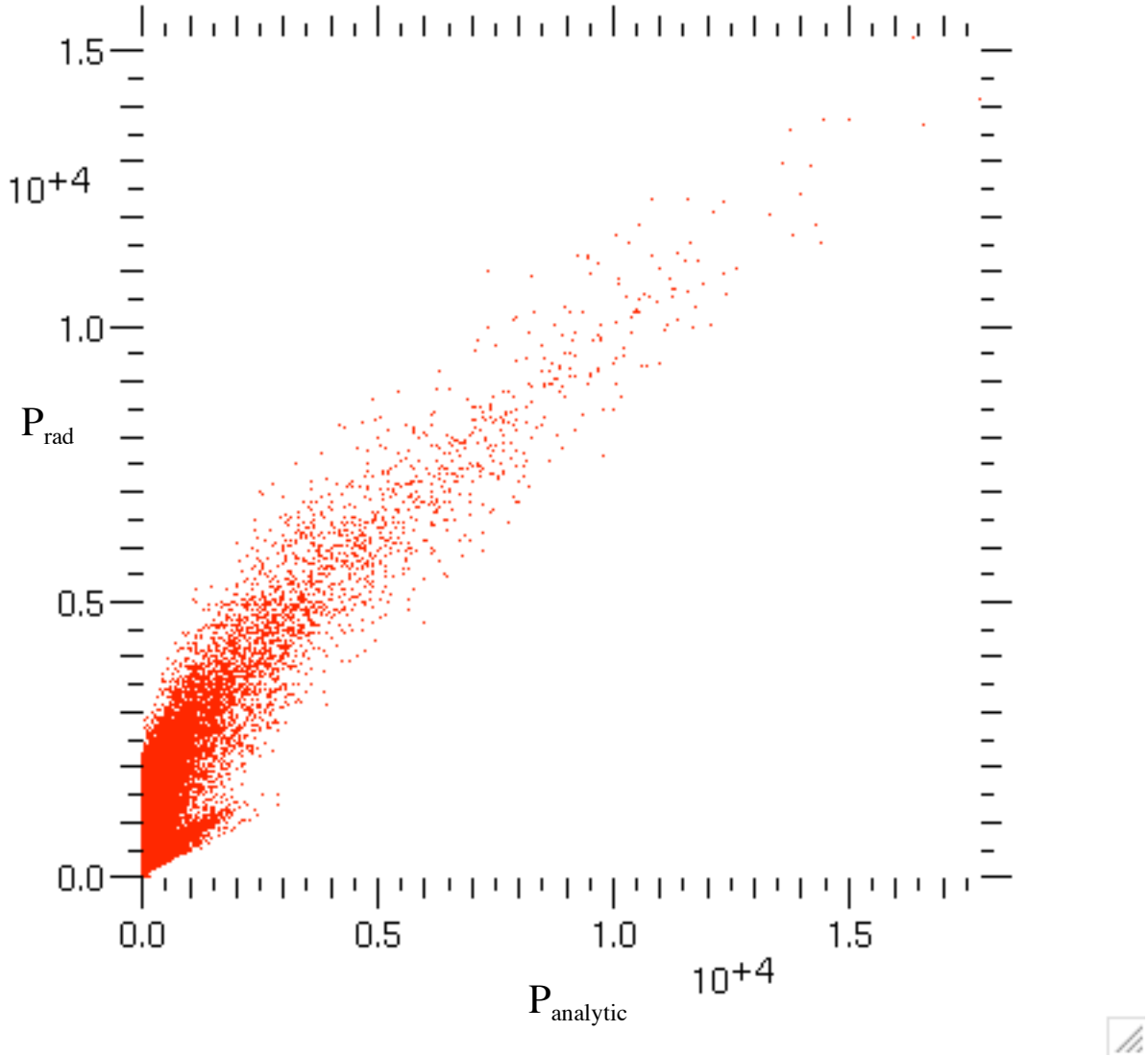

Fig1

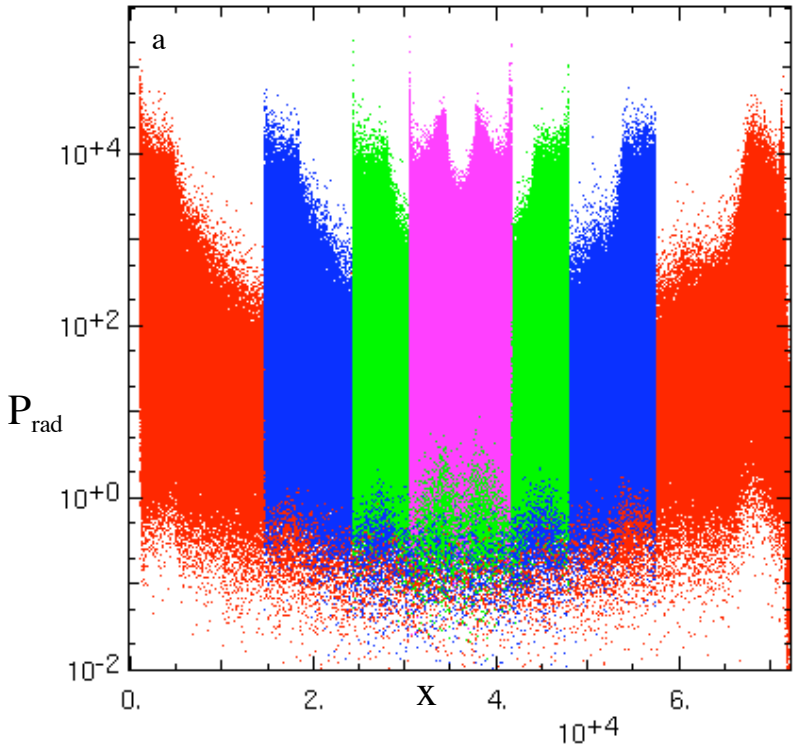

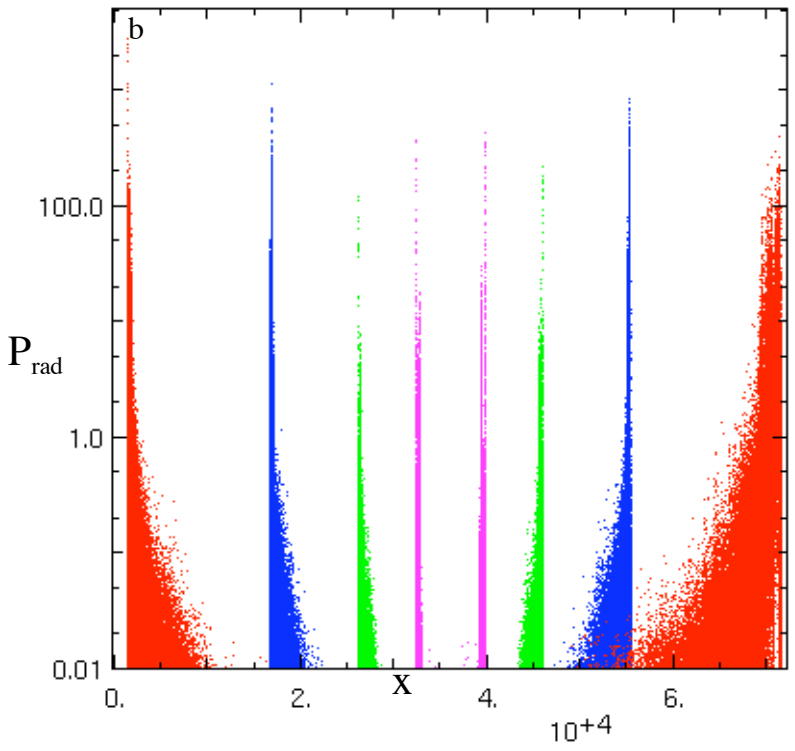

Fig2

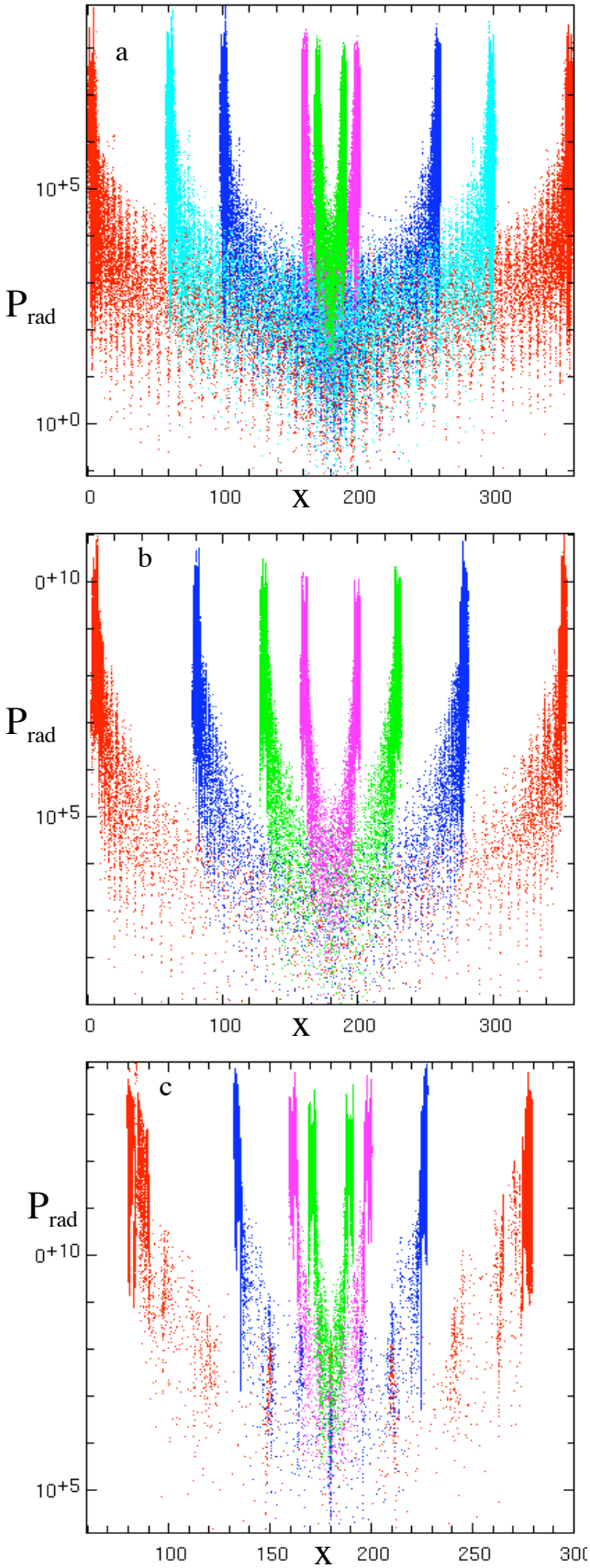
a
10^{+5}
P_{rad}
10^{+0}
0
100
X
200
300
b
0^{+10}
P_{rad}
10^{+5}
0
100
X
200
300
c
P_{rad}
0^{+10}
10^{+5}
100
150
X
200
250
300

Fig.3

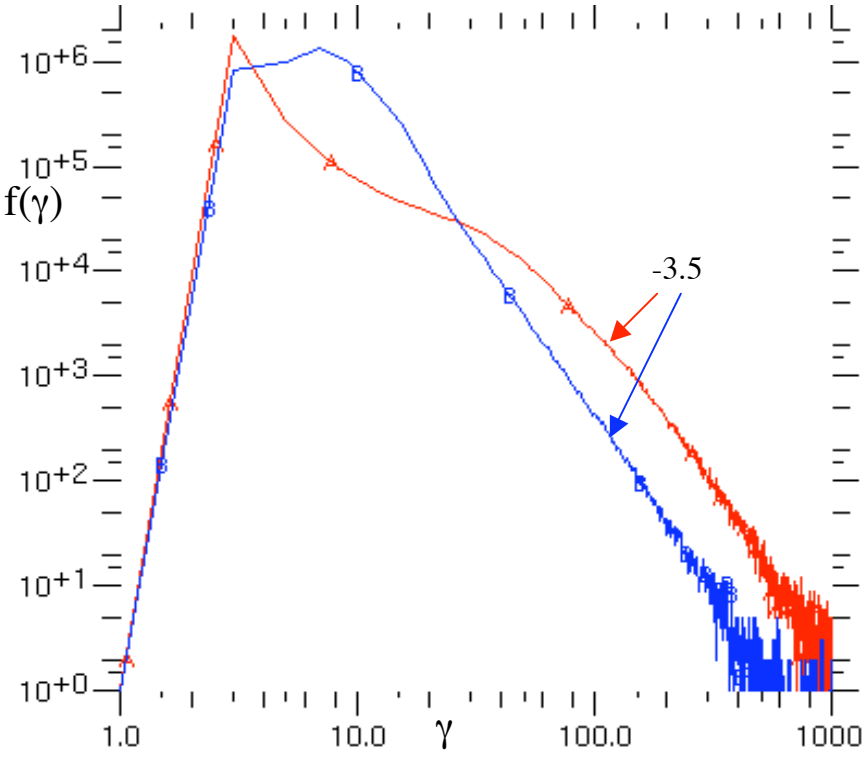

Fig.4

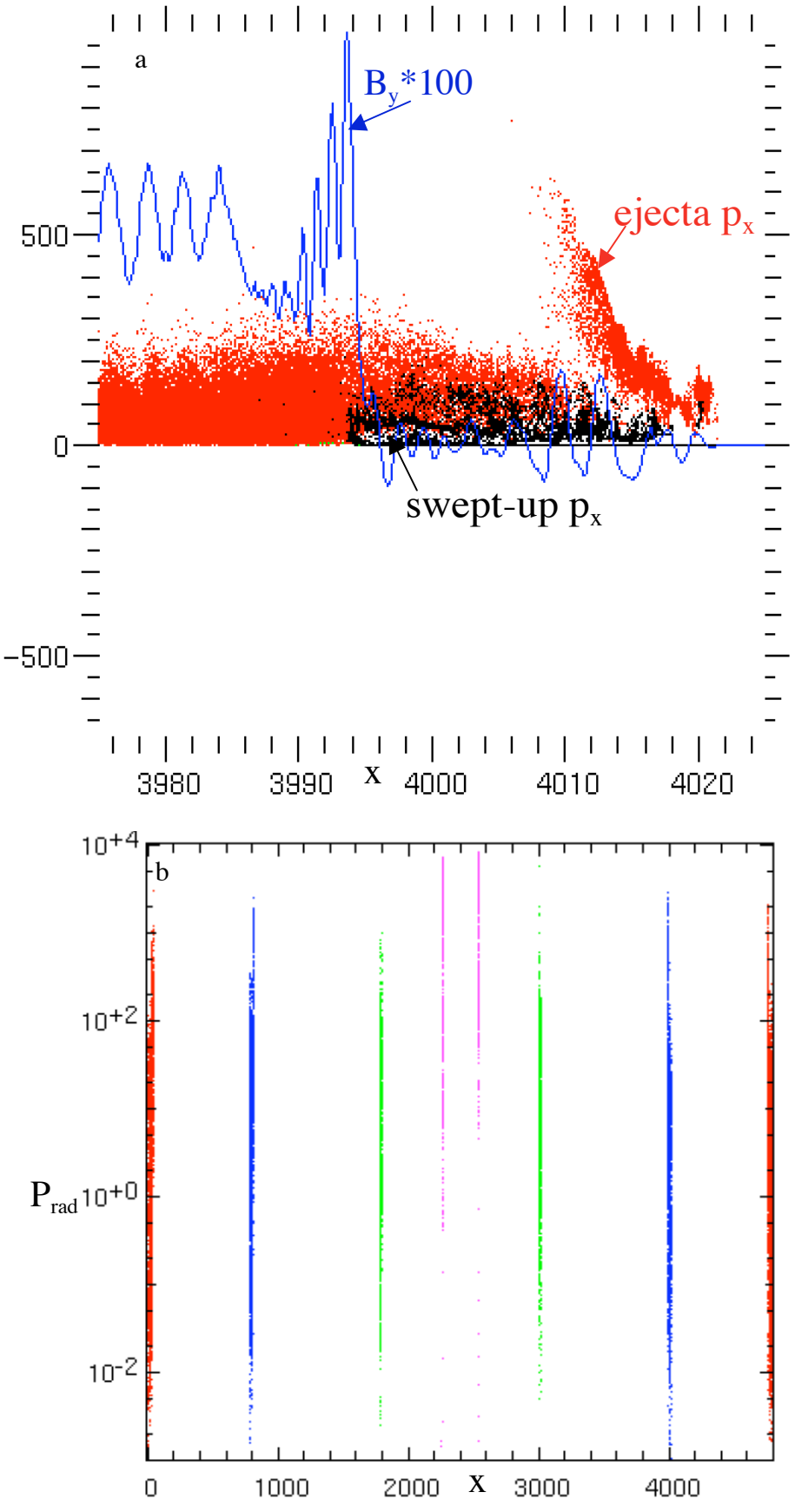
a
B_y*100
ejecta p_x
swept-up p_x
500
0
−500
3980
3990
x
4000
4010
4020
b
10^{+4}
10^{+2}
10^{+0}
10^{-2}
P_{rad}
0
1000
2000
x
3000
4000

Fig.5

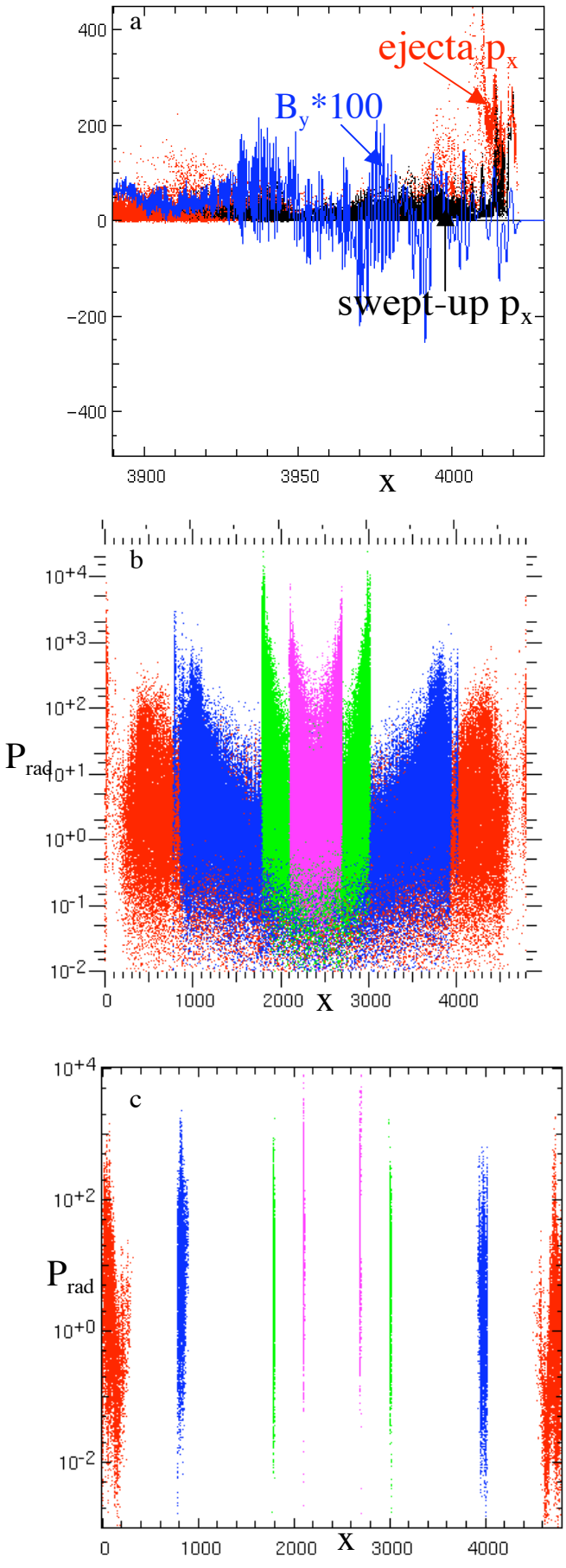
a
ejecta p_x
B_y*100
swept-up p_x
400
200
0
−200
−400
3900
3950
4000
x
b
P_{rad}
10^{+4}
10^{+3}
10^{+2}
10^{+1}
10^{+0}
10^{-1}
10^{-2}
0
1000
2000
3000
4000
x
c
P_{rad}
10^{+4}
10^{+2}
10^{+0}
10^{-2}
0
1000
2000
3000
4000
x

Fig.6